CrossMark

Whole-brain changes in white matter microstructure after radiotherapy for nasopharyngeal carcinoma: a diffusion tensor imaging study

Fuhong Duan[1,2] · Jingliang Cheng[1] · Jianwei Jiang[3] · Jun Chang[3] ·
Yong Zhang[1] · Shijun Qiu[2]

Abstract Radiation-induced local white matter (WM) damage has been observed by diffusion tensor imaging (DTI) within a priori-defined regions of interest following radiotherapy (RT) for nasopharyngeal carcinoma (NPC). In this study, we aimed to detect WM changes throughout the brain of NPC patients by DTI. Tract-based spatial statistics (TBSS) was used to analyze DTI data from 81 NPC patients. Fractional anisotropy (FA) and mean diffusivity (MD) were quantified across the whole brain in separate groups: pre-RT, and <6, 6–12, and >12 months post-RT. We found that fractional anisotropy values were significantly lower in the right frontal, parietal, and occipital WM <6 months post-RT compared with pre-RT and remained significantly lower in the right frontal and parietal WM at >12 months. MD values were significantly higher in the right occipital, bilateral temporal, right occipital–temporal junction, left parietal, left centrum semiovale, and left frontal–parietal junction WM <6 months post-RT and remained higher in the right occipital WM at >12 months. This study suggests that changes in white matter microstructure following RT for NPC were widespread,

complex, and dynamic. Diffusion tensor imaging with TBSS analysis allows for early non-invasive detection of RT-induced WM damage.

Introduction

Radiation therapy (RT) is the current treatment of choice for nasopharyngeal carcinoma (NPC). However, RT not only kills tumor cells but also damages adjacent tissue, especially the lower temporal lobes, because they are within the RT target volume. Radiation-induced brain injury (RBI) is a major neurologic complication following RT for NPC, negatively impacting prognosis and quality of life [1]. The prevalence of radiation-induced brain injury ranges from 4 to 18 % [2]. The typical brain response to RT has been divided into three phases based on the timing of symptom onset. Both the acute effects occurring during the first weeks following RT and early delayed or subacute effects typically appearing 1–6 months after completion of RT are generally reversible, while the late delayed effects appearing more than 6 months after RT are generally irreversible and even progressive [3–5].

Magnetic resonance (MR) diffusion tensor imaging (DTI) is currently the only noninvasive imaging modality for characterizing subtle changes in white matter (WM) microstructure in vivo [6, 7]. Diffusion tensor imaging provides a measure of water diffusion within each voxel as expressed by mean diffusion (MD) and direction dependence of diffusion (or fractional anisotropy, FA). These metrics can be used to construct images of nerve fiber

F. Duan and J. Cheng contributed equally to the article.

✉ Shijun Qiu
qiushijun001@163.com

[1] Department of MRI, The First Affiliated Hospital of Zhengzhou University, No. 1, Jianshe East Road, Zhengzhou 450052, People's Republic of China

[2] Department of Medical Imaging Center, The first affiliated hospital of Guangzhou University of Chinese Medicine, 16# Jichang Road, Guangzhou 510405, People's Republic of China

[3] Department of Radiology, The Third Affiliated Hospital of Nantong University, No. 585, Xingyuan North Road, Wuxi 214041, People's Republic of China

pathways (tractography) and estimate changes in fiber numbers and myelination during development and disease [7]. In general, lower FA and higher MD suggest disruption of fiber integrity. Recent studies have revealed that DTI can be used for early detection of localized radiation-induced damage in brain parenchyma following RT, even if there are no visible lesions on conventional MR images [8–13]. However, these studies investigated only alterations in local WM fiber integrity within prespecified regions of interest (ROI). Tract-based spatial statistics (TBSS) is an observer-independent approach for accurate and automatic analysis of DTI data that can detect group-wise microstructural differences in the major WM pathways of the brain [14]. Also, TBSS analysis of DTI data does not require smoothing and has more precise alignment [15]. In vivo tractography may reveal changes in WM associated with the early stages of neurological and psychiatric disorders, thereby aiding in diagnosis and treatment.

In this study, we used DTI and TBSS to compare white matter (WM) microstructure at different times after RT in NPC patients.

Materials and methods

Subjects

Eighty-one NPC patients (mean age 44.26 ± 9.91 years, range 19–65 years, 21 females) were enrolled and divided into four groups according to the time before and after completion of RT: G1 (pre-RT, $n = 23$), G2 (0–6 months post-RT, $n = 21$), G3 (>6–12 months post-RT, $n = 20$), and G4 (>12 months post-RT, $n = 17$), matched on age, gender ratio, and education level (Table 1).

All NPC patients were confirmed pathologically, with staging from T1N0M0 to T4N2M0 (Union for International Cancer Control, Seventh Edition, 2009) (Table 2). No patient had previously been treated by RT. The primary tumor and the upper neck above the caudal edge of the cricoid cartilage were treated with intensity-modulated radiation therapy (IMRT) techniques. According to International Commission on Radiation Units and Measurements (ICRU) reports 50, 62, and 83, we contoured the

gross target volume (GTV), clinical target volume (CTV), and organs at risk (OARs) on sectional CT or MRI. A 3-mm margin was used to generate the corresponding planning target volume and planning organs at risk volume (PTV/PRV) with necessary modifications. The prescribed dose of gross tumor volume of the primary (GTV-P) was 66–74 Gy, gross tumor volume of cervical lymph nodes metastased (GTV-N) was 64–68 Gy, CTV l (i.e., high-risk regions) was 56–60 Gy, and CTV 2 (i.e., low-risk regions) and CTV-N (i.e., cervical nodal regions) was 50–54 Gy. The daily dose of irradiation was 1.8–2.0 Gy (5 days a week), which was carried out with a linear accelerator (linac; 6 MV X-rays; Elekta Synergy). In all patients, 59 patients received concurrent chemotherapy, and 22 received adjuvant chemotherapy. The concurrent chemotherapy regimen was consisting of five to six cycles of injection cisplatin (CDDP; 40 mg/m^2) weekly. Among patients receiving three to four cycles of adjuvant chemotherapy, seventeen received CDDP(75 mg/m^2) on day 1 and 5-fluorouracil (5-FU; 500 mg/m^2) on days 1–5, and five patients were treated with CDDP and docetaxel (both dosed at 75 mg/m^2) on day 1, and these cycles were repeated every 3 weeks. We contoured the OARs, such as the brain stem, spinal cord, temporal lobe, eye, lens, optic nerve, chiasm, salivary glands, temporomandibular joint, mandible, and so on, according to their three-dimensional

Table 2 TNM stage of nasopharyngeal carcinoma patients

Stage	No. of patients	%
T stage		
1	12	14.8
2	20	24.7
3	34	42.0
4	15	18.5
N stage		
0	14	17.3
1	19	23.5
2	48	59.2
UICC stage		
I	3	3.7
II	15	18.5
III	48	59.3
IV$_A$	15	18.5

Table 1 Demographic and clinical characteristics of nasopharyngeal carcinoma patients

Characteristics	G1 (Pre-RT) ($n = 23$)	G2 (0–6 m) ($n = 21$)	G3 (>6–12 m) ($n = 20$)	G4 (>12 m) ($n = 17$)	F/χ^2 value	P value
Age (years)	47.04 ± 9.56	41.48 ± 12.40	41.75 ± 7.62	46.88 ± 8.24	1.407	0.237
Male/female	18/5	13/8	16/4	13/4	2.417	0.660
Education (years)	9.91 ± 3.40	10.48 ± 3.53	10.45 ± 3.32	10.29 ± 3.12	0.098	0.983

Pre-RT before radiotherapy, m months

anatomical boundaries on CT–MRI fusion. The whole organs should be outlined, including those in CTV, but not GTV. According to the Radiation Therapy Oncology Group (RTOG) 0615 and 0225, the limiting dose of the organs at risk was set as follow: brain stem ≤54 Gy, spinal cord ≤45 Gy, temporal lobe ≤54–60 Gy, optic nerve and chiasm ≤54 Gy, lens ≤9 Gy, D50 of parotid gland ≤30–35 Gy, temporomandibular joint ≤50 Gy, and mandible ≤60 Gy. Exclusion criteria were age less than 18 or greater than 65 years, intracranial primary tumors or metastases, intracranial invasion, neurovascular lesions, head trauma, previous intracranial surgery, hypertension, heart disease, diabetes, hyperlipidemia, metabolic disease, major psychiatric or neurological disorders, left-handedness, the existence of brain abnormalities on conventional or enhanced MRI, and contraindications to scanning.

Image acquisition

All MR imaging data were acquired using a 3.0 T GE clinical scanner (SIGNA EXCITE GE Medical Systems, Milwaukee, WI, USA) with an eight-channel head coil. The routine MRI brain protocol included T1-weighted, T2-weighted, and T2-FLAIR images for every subject to detect intracranial lesions. Diffusion tensor imaging scans employed a single-shot echo-planar imaging sequence and array spatial sensitivity encoding technique with the following parameters: repetition time (TR) 12,000 ms, echo time (TE) 75.5 ms, field of view (FOV) 240 mm^2, matrix 128 × 128, slice thickness 2 mm, NEX = 1, and flip angle of 90°. Images were collected along 25 non-collinear diffusion gradient directions with b values of 1000 and 0 s/mm^2 (non-diffusion weighted).

Data processing and TBSS analysis

The FMRIB Software Library (FSL, http://www.fmrib.ox.ac.uk/fsl, version 4.19) was used for preprocessing DTI data. First, diffusion tensor images were corrected for head movements and eddy current distortion using the FDT tool. Second, a binary brain mask was obtained for each participant from the respective $b = 0$ image using the BET tool. The diffusion tensor was then calculated voxel by voxel using dtifit to generate maps of fractional anisotropy (FA) and mean diffusivity (MD).

Voxel-wise analysis of multisubject diffusion data was performed using TBSS as follows. (1) Original FA data were converted into the appropriate format. (2) All FA images were transformed into Montreal Neurological Institute (MNI) space by nonlinear registration. (3) We created the mean FA image and the skeletonized mean FA image using an FA threshold of 0.2. (4) We projected all subject FA images onto the mean FA skeleton. (5) Voxel-wise statistics on multisubject FA data were then computed in the skeleton space. Areas of statistically significant difference ($P < 0.05$) among the different groups were identified and corrected for multiple comparisons by family wise error correction (FWE) with threshold-free cluster enhancement [16].

Statistical analyses

Data were analyzed using the Statistical Package for Social Sciences 13.0 (SPSS for Windows, Chicago, IL, USA). One-way analysis of variance (ANOVA) was performed to compare age and years of education among the different groups. The Chi-square test was performed to assess differences in gender ratio. A two-tailed P value <0.05 was considered statistically significant.

Results

Demographic data

There were no significant differences in age, gender ratio, and duration of education among groups (G1–G4) (Table 1).

Changes in fractional anisotropy (FA)

Compared with the pre-RT group (G1), FA was significantly lower in the right frontal, parietal, and occipital WM in NPC patients assessed within 6 months after RT (G2) (Fig. 1; Table 3). While values increased gradually thereafter, FA remained significantly lower in the right frontal and parietal WM in NPC patients evaluated by DTI >12 months post-RT (G4) compared with the pre-RT group (Table 4).

Changes in mean diffusibility (MD)

Compared with the pre-RT group, MD values in the right occipital, bilateral temporal, right occipital–temporal junction area, left parietal, left centrum semiovale, and left frontal–parietal junction area WM were significantly higher within 6 months post-RT (Fig. 2; Table 5). Values decreased thereafter in most regions but were still elevated in the right occipital WM in the >12 months post-RT group compared with the pre-RT group (Table 6).

Discussion

Radiation therapy effectively destroys cancerous tissues, but may also damage adjacent healthy tissue, a particularly severe adverse effect in tissues with limited
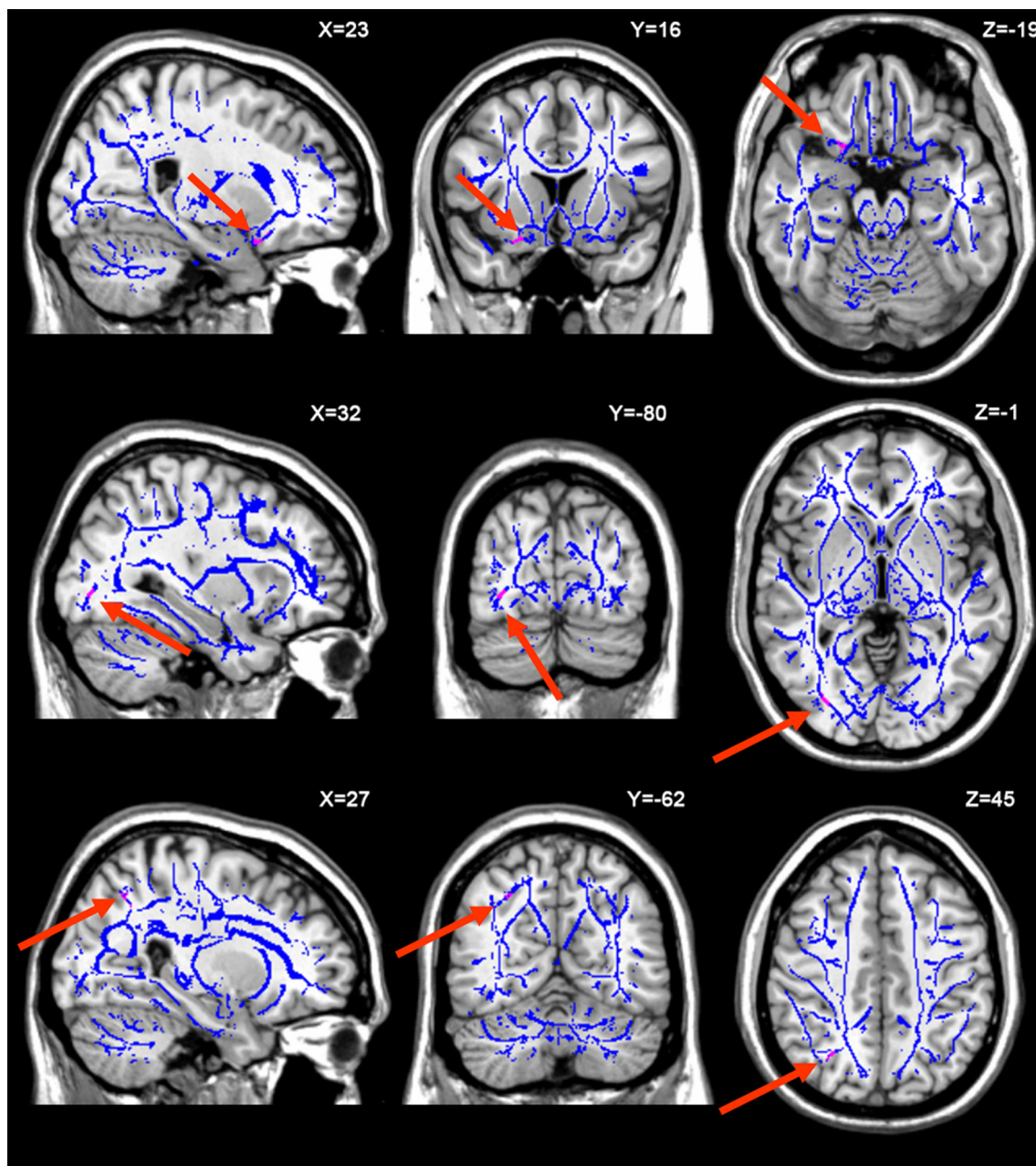
Fig. 1 Differences in fractional anisotropy (FA) values between the 0–6 months post-radiotherapy (RT) group and the pre-RT group of nasopharyngeal carcinoma (NPC) patients. Areas in *blue* exhibit no significant difference in FA by group-wise comparison. *Red* areas denote regions of significantly lower FA (*red arrows*) in the 0–6 months post-RT group compared with the pre-RT group. *Arabic numerals* indicate the location of each section in Montreal Neurological Institute (MNI) coordinates

regenerative capacity, such as the adult mammalian central nervous system. In contrast to DTI and TBSS analysis, most conventional neuroimaging modalities are of limited value for assessing early abnormalities of the microstructure of white matter due to radiotherapy. To the best of our knowledge, this is the first study to investigate changes in whole-brain WM microstructure after radiotherapy (RT) using DTI and TBSS in nasopharyngeal carcinoma patients. Patients showed

radiation-induced brain injury involving regions of normal-appearing WM beyond the target field. Furthermore, these abnormalities were most severe within 6 months after radiotherapy, and different brain regions exhibited distinct rates of recovery thereafter.

In accordance with previous DTI studies [9, 10], DTI indices were found significantly changed in the temporal WM, very likely because subregions of the temporal lobe are closer to the nasopharyngeal target volume and are

Table 3 Brain regions with abnormal FA values in the 0–6 months post-RT group compared with the pre-RT group ($P < 0.05$, FWE corrected)

Brain regions	L/R	Voxels	MNI coordinates (mm)			Peak t score	P value
			X	Y	Z		
Lower FA							
Frontal WM	R	55	23	16	−19	5.5277	<0.0001
Occipital WM	R	57	32	−80	−1	5.9544	<0.0001
Parietal WM	R	65	27	−62	45	4.5864	<0.0001

L left, *R* right, *MNI* Montreal Neurological Institute

Table 4 Brain regions with abnormal FA values more than 12 months post-RT group compared with the pre-RT group ($P < 0.05$, FWE corrected)

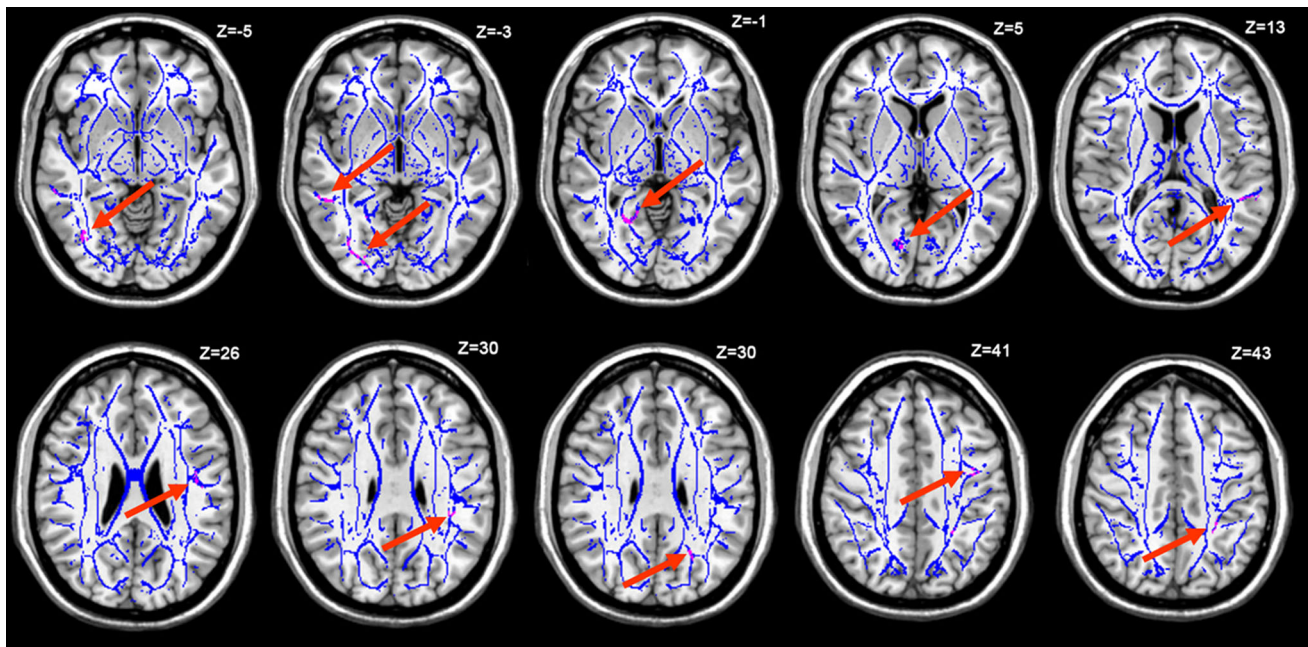| Brain regions	L/R	Voxels	MNI coordinates (mm)			Peak t score	P value
			X	Y	Z		
Lower FA							
Frontal WM	R	55	23	16	−19	2.5155	0.0162
Parietal WM	R	65	27	−62	45	2.4543	0.0188

Fig. 2 Differences in mean diffusivity (MD) values between the 0–6 months post-RT group and the pre-RT group of NPC patients. Areas in *blue* show no significant difference by group-wise comparison. *Red* areas exhibit significantly higher MD values (*red arrows*) in the 0–6 months post-RT group compared with the pre-RT group

inevitably encompassed in the radiation field, which causes a radiation dose that may exceed the tolerance limit of neural tissue. Also, TBSS analysis revealed significant changes in DTI indices in parietal, frontal, occipital, and cerebellar WM regions well beyond the irradiation zone. This damage outside the irradiation zone may arise from radiation-induced cerebrovascular injury with ensuing ischemia or metabolic disruption, autoimmune vasculitis [17, 18], cellular oxidative stress and membrane lipid peroxidation [19], and (or) release of diffusible neurotoxins

that can trigger demyelination or fiber dysfunction of distant tissues [20].

The fractional anisotropy, a normalized measure of anisotropy calculated from the diffusion tensor, is sensitive to microstructural changes in WM integrity [21]. A higher FA often reflects greater fiber density, more numerous fibers, more myelinated fibers, and (or) more coherent fiber orientation. MD should be interpreted in terms of changes of the diffusion coefficient in the extracellular space, which reflects overall diffusivity. Increased MD indicates more

Table 5 Brain regions with abnormal MD values 0–6 months post-RT group compared with the pre-RT group ($P < 0.05$, FWE corrected)

Brain regions	L/R	Voxels	MNI coordinates (mm)			Peak t score	P value
			X	Y	Z		
Higher MD							
Occipital WM	R	127	30	−82	−3	−5.9456	<0.0001
Occipital WM	R	69	37	−75	−5	−3.6101	0.0008
Temporal WM	R	74	52	−43	−3	−5.8621	<0.0001
Occipital–temporal junction area	R	64	23	−54	−1	−4.9454	<0.0001
Occipital WM	R	94	17	−72	5	−4.6469	<0.0001
Temporal WM	L	88	−46	−43	13	−6.3585	<0.0001
Parietal WM	L	57	−37	−34	30	−4.7024	<0.0001
Centrum semiovale	L	67	−42	−14	26	−5.9277	<0.0001
Frontal–parietal junction area	L	97	−40	−5	41	−5.2751	<0.0001
Parietal WM	L	62	−23	−59	30	−3.7421	0.0005
Parietal WM	L	66	−26	−46	43	−5.3720	<0.0001

Table 6 Brain regions with abnormal MD values more than 12 months post-RT group compared with the pre-RT group ($P < 0.05$, FWE corrected)

Brain region	L/R	Voxels	MNI coordinates (mm)			Peak t score	P value
			X	Y	Z		
Higher MD							
Occipital WM	R	69	37	−75	−5	−2.0772	0.0446

free water molecules contained in the brain tissues. In the present study, FA was lower in the WM underlying the right frontal, parietal, and occipital lobes and MD values were significantly higher in the right occipital, bilateral temporal, right occipital–temporal junction, left parietal, left centrum semiovale, and left frontal–parietal junction WM within the first 6 months following RT. Consistent with previous studies [8, 22–24], these changes recovered gradually, but FA remained lower in the right frontal and parietal WM, and MD remained higher in the right occipital WM for over 1 year. The lower FA and higher MD observed in normal-appearing WM within 6 months after RT may reflect transient cerebral edema and demyelination, while the ensuing reversals may be due to recovery from edema, oligodendrocyte regeneration, clearance of debris by inflammatory cells, and ultimate remyelination [13, 25–27]. Alternatively, the sustained decrease in FA within the right frontal and parietal WM and the sustained increase in MD in the right occipital WM may represent permanent damage. However, much additional work is required to reliably correlate DTI results with specific pathophysiological processes induced by brain irradiation.

This study has several limitations. First, the spatial resolution of TBSS limits analysis to major WM tracts and is insufficient to detect fine changes in regional WM structure. Therefore, higher resolution voxel-based approaches across the whole brain are needed to validate our results. Second, we did not monitor the effects of chemotherapeutics, which could potentially influence in FA and MD of white matter tracts, not all the patients received the same scheme of chemotherapy. Radiotherapy, combined with chemotherapy, can improve the survival rate of patients with advanced nasopharyngeal carcinoma. However, there have been a few long-term follow-up studies on the impact of chemotherapy on brain structure and function. Further study with a larger population is warranted.

In conclusion, we employed DTI and TBSS to investigate changes in whole-brain white matter properties at different time points after radiotherapy for NPC. The effects of radiation on the microstructure of WM were generally transient but involved multiple brain regions beyond the irradiation focus. In vivo measurements of WM integrity using DTI may facilitate early detection of radiation-induced brain damage in NPC patients, allowing for therapeutic modifications to reduce the risk of irreversible brain radiation injury.

Compliance with ethical standards

Conflict of interest The authors declare that they have no conflict of interest.

Ethical approval All procedures performed in studies involving human participants were in accordance with the ethical standards of the institutional research committee and with the 1964 Helsinki declaration and its later amendments or comparable ethical standards.

Informed consent Informed consent was obtained from all individual participants included in the study.

References

1. Lee AW, Law SC, Ng SH, Chan DK, Poon YF, Foo W, Tung SY, Cheung FK, Ho JH (1992) Retrospective analysis of nasopharyngeal carcinoma treated during 1976–1985: late complications following megavoltage irradiation. Br J Radiol 65:918–928

2. Valk PE, Dillon WP (1991) Radiation injury of the brain. AJNR Am J Neuroradiol 12:45–62

3. Shanmugaratnam K, Chan SH, De-The G, Goh JE, Khor TH, Simons MJ, Tye CY (1979) Histopathology of nasopharyngeal carcinoma: correlations with epidemiology, survival rates and other biological characteristics. Cancer 44:1029–1044

4. New P (2001) Radiation injury to the nervous system. Curr Opin Neurol 14:725–734

5. Laack NN, Brown PD (2004) Cognitive sequelae of brain radiation in adults. Semin Oncol 31:702–713

6. Basser PJ, Pierpaoli C (1998) A simplified method to measure the diffusion tensor from seven MR images. Magn Reson Med 39:928–934

7. Johansen-Berg H, Behrens TE (2006) Just pretty pictures? What diffusion tractography can add in clinical neuroscience. Curr Opin Neurol 19:379–385

8. Welzel T, Niethammer A, Mende U, Heiland S, Wenz F, Debus J, Krempien R (2008) Diffusion tensor imaging screening of radiation-induced changes in the white matter after prophylactic cranial irradiation of patients with small cell lung cancer: first results of a prospective study. AJNR Am J Neuroradiol 29:379–383

9. Wang HZ, Qiu SJ, Lv XF, Wang YY, Liang Y, Xiong WF, Ouyang ZB (2012) Diffusion tensor imaging and 1H-MRS study on radiation-induced brain injury after nasopharyngeal carcinoma radiotherapy. Clin Radiol 67:340–345

10. Xiong WF, Qiu SJ, Wang HZ, Lv XF (2013) (1) H-MR spectroscopy and diffusion tensor imaging of normal-appearing temporal white matter in patients with nasopharyngeal carcinoma after irradiation: initial experience. J Magn Reson Imaging 37:101–108

11. Trivedi R, Khan AR, Rana P, Haridas S, Hemanth KB, Manda K, Rathore RK, Tripathi RP, Khushu S (2012) Radiation-induced early changes in the brain and behavior: serial diffusion tensor imaging and behavioral evaluation after graded doses of radiation. J Neurosci Res 90:2009–2019

12. Laitinen T, Sierra A, Pitkanen A, Grohn O (2010) Diffusion tensor MRI of axonal plasticity in the rat hippocampus. Neuroimage 51:521–530

13. Wang S, Wu EX, Qiu D, Leung LH, Lau HF, Khong PL (2009) Longitudinal diffusion tensor magnetic resonance imaging study of radiation-induced white matter damage in a rat model. Cancer Res 69:1190–1198

14. Zhuang L, Wen W, Zhu W, Trollor J, Kochan N, Crawford J, Reppermund S, Brodaty H, Sachdev P (2010) White matter integrity in mild cognitive impairment: a tract-based spatial statistics study. Neuroimage 53:16–25

15. Smith SM, Jenkinson M, Johansen-Berg H, Rueckert D, Nichols TE, Mackay CE, Watkins KE, Ciccarelli O, Cader MZ, Matthews PM, Behrens TE (2006) Tract-based spatial statistics: voxel-wise analysis of multi-subject diffusion data. Neuroimage 31:1487–1505

16. Smith SM, Nichols TE (2009) Threshold-free cluster enhancement: addressing problems of smoothing, threshold dependence and localisation in cluster inference. Neuroimage 44:83–98

17. Xavier S, Piek E, Fujii M, Javelaud D, Mauviel A, Flanders KC, Samuni AM, Felici A, Reiss M, Yarkoni S, Sowers A, Mitchell JB, Roberts AB, Russo A (2004) Amelioration of radiation-induced fibrosis: inhibition of transforming growth factor-beta signaling by halofuginone. J Biol Chem 279:15167–15176

18. Ramanan S, Zhao W, Riddle DR, Robbins ME (2010) Role of PPARs in radiation-induced brain injury. PPAR Res 2010:234975

19. Kim JH, Brown SL, Jenrow KA, Ryu S (2008) Mechanisms of radiation-induced brain toxicity and implications for future clinical trials. J Neurooncol 87:279–286

20. Crossen JR, Garwood D, Glatstein E, Neuwelt EA (1994) Neurobehavioral sequelae of cranial irradiation in adults: a review of radiation-induced encephalopathy. J Clin Oncol 12:627–642

21. Mukherjee P, McKinstry RC (2006) Diffusion tensor imaging and tractography of human brain development. Neuroimaging Clin N Am 16:19–43

22. Nagesh V, Tsien CI, Chenevert TL, Ross BD, Lawrence TS, Junick L, Cao Y (2008) Radiation-induced changes in normal-appearing white matter in patients with cerebral tumors: a diffusion tensor imaging study. Int J Radiat Oncol Biol Phys 70:1002–1010

23. Kitahara S, Nakasu S, Murata K, Sho K, Ito R (2005) Evaluation of treatment-induced cerebral white matter injury by using diffusion-tensor MR imaging: initial experience. AJNR Am J Neuroradiol 26:2200–2206

24. Khong PL, Kwong DL, Chan GC, Sham JS, Chan FL, Ooi GC (2003) Diffusion-tensor imaging for the detection and quantification of treatment-induced white matter injury in children with medulloblastoma: a pilot study. AJNR Am J Neuroradiol 24:734–740

25. Harsan LA, Poulet P, Guignard B, Steibel J, Parizel N, de Sousa PL, Boehm N, Grucker D, Ghandour MS (2006) Brain dysmyelination and recovery assessment by noninvasive in vivo diffusion tensor magnetic resonance imaging. J Neurosci Res 83:392–402

26. Peiffer AM, Shi L, Olson J, Brunso-Bechtold JK (2010) Differential effects of radiation and age on diffusion tensor imaging in rats. Brain Res 1351:23–31

27. Li H, Li JP, Lin CG, Liu XW, Geng ZJ, Mo YX, Zhang R, Xie CM (2012) An experimental study on acute brain radiation injury: dynamic changes in proton magnetic resonance spectroscopy and the correlation with histopathology. Eur J Radiol 81:3496–3503